Effects of Laser Wavelength on Interaction of Ultrashort Intense Laser with Finite-Scale Length Dense Plasmas

Susumu KATO, Eiichi TAKAHASHI, Yuji MATSUMOTO and Isao OKUDA

National Institute of Advanced Industrial Science and Technology (AIST), Tsukuba 305-8568, Japan

(Received 25 May 2007 / Accepted 13 June 2007)

The energetic electrons and ions generated by the interaction of an intense, ultrashort laser pulse with a finite scale-length dense plasma were investigated for various laser wavelengths using particle-in-cell simulation. The hot-electron temperature for the density scale-length $L = 2.5\,\mu\text{m}$ is not governed by the $I\lambda^2$-scaling laws, where I is the laser intensity and λ is the laser wavelength. The maximum energy of the energetic ions is not only proportional to the hot-electron temperature but depends on the electron density.

Keywords: ultraintense laser, energetic electron production, energetic ion production, laser-plasma interactions

DOI: 10.1585/pfr.2.032

Energetic electron and ion beam production from ultrashort intense laser-plasma interactions shows promise for application in radioisotope production for positron emission tomography [1, 2]. The experiments in this work employed an infrared subpicosecond laser, e.g., a Nd:glass laser ($\lambda = 1053$ nm) or a Ti:sapphire laser ($\lambda = 800$ nm) for two main reasons. The first reason is technical: it is difficult to produce an ultraintense laser with other wavelengths. However, KrF laser systems ($\lambda = 248$ nm) could produce irradiance intensities of the order of 10^{18} W/cm^2 [3, 4]. The second reason is due to the $I\lambda^2$-scaling laws [5], where I is the laser intensity and λ is the laser wavelength. The $I\lambda^2$-scaling laws indicate an advantage in using long wavelength lasers to generate energetic particles. In our previous paper [6, 7], we stated that the interaction of intense laser pulses with solid-density plasmas is not governed solely by the $I\lambda^2$-scaling laws.

Typically, an ultrashort intense laser pulse has a prepulse or pedestal. Therefore, a controlled or uncontrolled underdense preplasma forms in front of a solid-density target before the main pulse arrives at the target surface. The scale length of the underdense preplasma strongly influences the energetic electrons produced by the laser-plasma interaction [8].

In this study, we investigate the interaction of an intense ultrashort laser pulse with finite scale-length dense plasmas at normal incidence, using one dimensional particle-in-cell (1D PIC) simulation code [9]. The effects of various laser wavelengths on laser absorption and energetic electron and ion production are characterized.

In the simulation, the parameters used for the laser pulse were as follows: a sine-squared envelope with a duration of 400 fs (i.e. the width at half maximum is 200 fs), irradiated intensity $I = 5 \times 10^{18}$ W/cm^2, and three different wavelengths $\lambda = 0.25$, 0.5, and 1 μm. The schematic of the density profile used in the PIC code is shown in Fig. 1. A thin target is expressed by an ion density of 1×10^{22} cm^{-3}, mass number $A = 100$, and effective charge $Z = 10$ with a thickness of 0.3 μm. Preformed plasma sets are positioned at the front of the laser incidence. The preformed plasma, where $A = 12$ and $Z = 6$, has temperature 1 keV and an exponentially decreasing density profile $n_0 \exp(-x/L)$, where $n_0 = 2 \times 10^{22}$ cm^{-3} is the electron density at the interface between the thin target and preformed plasma, and L is the scale length of the preformed plasma. The scale length is varied from $L = 1$-2.5 μm. Protons are positioned behind the rear surface to investigate ion acceleration because of a high-energy electron sheath formed at the rear surface [10]. The protons have a density and thickness of 1×10^{22} cm^{-3} and 0.1 μm, respectively.

At all laser wavelengths and scale lengths, the laser pulse interacts with the preformed plasmas at a critical density, this implies, the pulse does not interact with the solid target. The interaction point varies with the wavelength, and the critical density for $\lambda = 0.25$ μm is 16 times higher than that for $\lambda = 1$ μm.

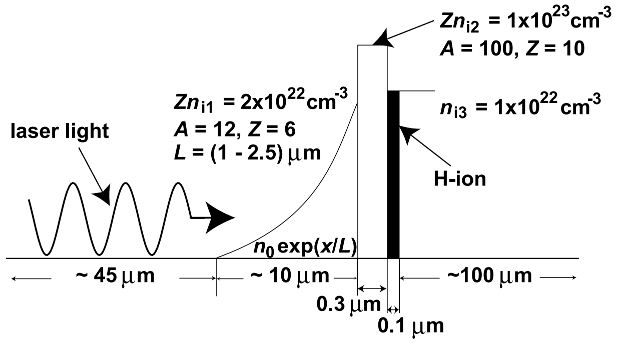

Fig. 1 Schematic of the density profile used in the particle-in-cell code.

author's e-mail: s.kato@aist.go.jp

Table 1 Laser absorption fraction as a function of the scale length L and laser wavelength λ.

scale length	laser wavelength (μm)		
(μm)	0.25	0.5	1.0
1.0	7.33%	7.25%	11.5%
1.5	12.2%	9.79%	13.0%
2.0	15.4%	12.4%	13.0%
2.5	21.6%	15.7%	13.2%

Table 1 gives the absorption fraction as a function of scale length and laser wavelength. For $\lambda = 1\,\mu$m, the absorption fraction is approximately constant while the normalized scale length L/λ increases from 1 to 2.5. For $\lambda = 0.25\,\mu$m, the absorption fraction triples while L/λ increases from 4 to 10. For $\lambda = 0.25\,\mu$m and $L = 2.5\,\mu$m, the absorption fraction is greater than 20%, even at normal incidence.

Electron-energy distributions after 215 fs, near the time of the laser-intensity peak, for $L = 2.5\,\mu$m are shown in Fig. 2. The hot-electron temperatures are 320, 500, and 500 keV, for $\lambda = 0.25$, 0.5, and 1 μm, respectively. The temperature of the hot electrons is estimated using the equation $T_{\mathrm{h}} \sim [(1 + I\lambda_{\mu}^2/1.4 \times 10^{18})^{1/2} - 1] \times 511$ keV [5], where I is the laser intensity in W/cm^2, and λ_{μ} is the wavelength in μm. For $\lambda = 1\,\mu$m, the measured temperature agrees with this estimation. However, for $\lambda = 0.25$ and 0.5 μm, the measured temperatures are higher than the estimation. Parametric processes at plasma densities below the quarter-critical density are involved in the principal mechanism instead of the mechanism originated from the ponderomotive potential. The number density around 500 keV for $\lambda = 0.25$ and 0.5 μm is about thrice that for $\lambda = 1\,\mu$m.

The energy distribution of the rear side proton after 415 fs, coinciding with the end of the laser pulse, for $L = 2.5\,\mu$m are shown in Fig. 3. The maximum proton energies are 4.7, 4.5, and 3.4 MeV for $\lambda = 0.25$, 0.5, and 1 μm, respectively. These results show the influence of high energy electron temperature and density on ion acceleration because of the sheath at the rear surface. The temperature of the energetic electron for $\lambda = 0.25\,\mu$m is no more than two thirds of that found at other wavelengths, while the density is about twice that for $\lambda = 0.5\,\mu$m, and thrice that for 1 μm. As a result, energetic ions are generated with energies comparable to the case for $\lambda = 0.5\,\mu$m, although the temperature of the high-energy electron is low.

This paper characterizes the effect of the different laser wavelengths on the temperature and density of energetic electrons created by the laser-plasma interaction using 1D-PIC simulation code. Multi-dimensional effects, such as surface deformation [5], are important in experiments. These simulations assume the ideal and collisionless plasma. In addition, electron transport in a solid-density target is affected by resistivity, which depends on the material used in experiments. Relatively low-energy electrons may be more strongly influenced by ambient plasma.

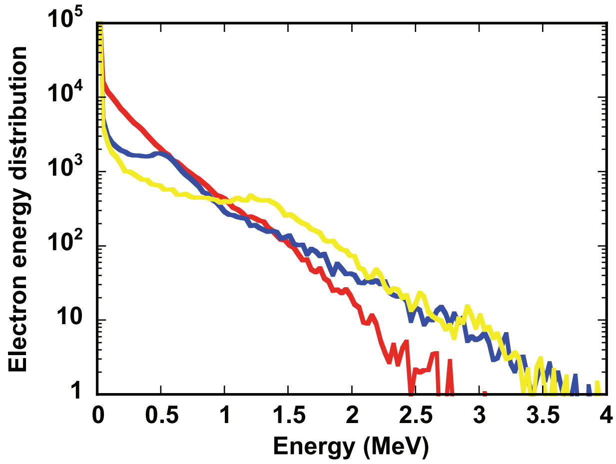

Fig. 2 Electron energy distribution at $t = 215$ fs. The red, blue, and yellow lines represent $\lambda = 0.25$, 0.5, and 1 μm, respectively.

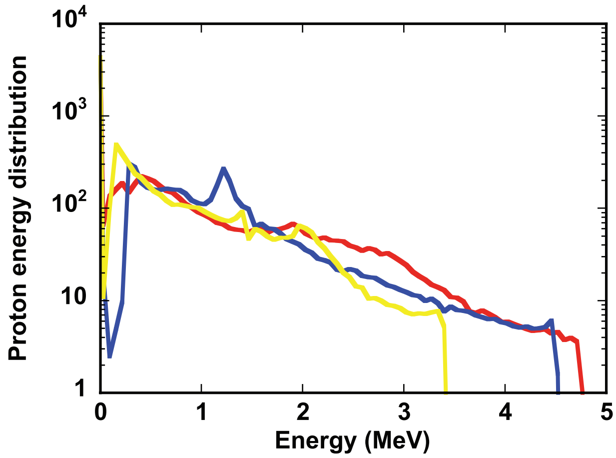

Fig. 3 Energy distribution of rear side proton at $t = 415$ fs. The red, blue, and yellow lines represent $\lambda = 0.25$, 0.5, and 1 μm, respectively.

This study was financially supported by the Budget for Nuclear Research of the Ministry of Education, Culture, Sports, Science and Technology, based on the screening and counseling by the Atomic Energy Commission.

[1] K. Nemoto *et al.*, Appl. Phys. Lett. **78**, 595 (2001).
[2] S. Fritzler *et al.*, Appl. Phys. Lett. **83**, 3039 (2003).
[3] U. Teubner *et al.*, Phys. Rev. E **54**, 4167 (1996).
[4] M. Borghesi *et al.*, Phys. Rev. E **60**, 7374 (1999).
[5] S.C. Wilks, Phys. Fluids B **5**, 2603 (1993); S.C. Wilks *et al.*, Phys. Rev. Lett. **69**, 1383 (1992).
[6] S. Kato *et al.*, J. Plasma Fusion Res. **78**, 717 (2002).
[7] S. Kato *et al.*, *Proc. of the 12th International Congress on Plasma Physics, 25-29 October 2004, Nice (France)*, http://hal.ccsd.cnrs.fr/ccsd-00001970
[8] E. Lefebvre and G. Bonnaud, Phys. Rev. E **55**, 1011 (1997).
[9] C.K. Birdsall and A.B. Langdon, *Plasma Physics via Computer Simulation* (McGraw-Hill, NewYork, 1985), Chap. 6.
[10] S.P. Hatchett *et al.*, Phys. Plasmas **7**, 2076 (2000).